CCS Chemistry

RESEARCH ARTICLE

Received: July 5, 2019 | Accepted: Jan. 4, 2020

Self-Assembly of Constrained Cyclic Peptides Controlled by Ring Size

Kuan Hu[1,3,4], Wei Xiong[2], Chengjie Sun[1], Chan Wang[4], Jingxu Li[1], Feng Yin[1,5], Yixiang Jiang[1], Ming-Rong Zhang[4], Zhou Li[3]*, Xinwei Wang[2]* & Zigang Li[1,5]*

[1]*State Key Laboratory of Chemical Oncogenomics, The School of Chemical Biology and Biotechnology, Peking University, Shenzhen Graduate School, Shenzhen 518055 (China),* [2]*School of Advanced Materials, Peking University, Shenzhen Graduate School, Shenzhen 518055 (China),* [3]*Beijing Institute of Nanoenergy and Nanosystems, Chinese Academy of Sciences, Beijing 100083 (China),* [4]*Department of Advanced Nuclear Medicine Sciences, The National Institute of Radiological Sciences, The National Institutes for Quantum and Radiological Science and Technology, Chiba, 263-8555 (Japan),* [5]*Pingshan Translational Medicine Center, Shenzhen Bay Laboratory, Shenzhen 518055 (China)*

**Corresponding authors: lizg@pkusz.edu.cn, wangxw@pkusz.edu.cn, zli@binn.cas.cn*

Cite this: *CCS Chem.* **2020**, *2*, 42–51

The de novo design of new peptide assemblies that expands the repertoire of biomaterial nanostructures has been of a tremendous challenge. Hence, it is evident that a successful research achievement in this area would increase the understanding of molecular interactions in supramolecules and create novel scaffolds exploitable in biotechnology and synthetic biology. The manipulation of cyclic peptide self-assembly is particularly intriguing for this purpose. Herein, we report that a novel type of cyclic peptides, referred to as chiral tether constrained cyclic peptides (CCP), shows promising self-assembly properties. CCPs are the first example of a controllable assembly of all-L-α-cyclic peptides with different ring sizes. A noteworthy feature of the CCP system is good tolerance of different secondary structures, ring size, and peptide sequence. Based on this system, a variety of nanostructures could be constructed, which display different physical properties, rendering it an excellent platform for molecular interaction studies. Further, demonstrate potential applications of these peptide assemblies in bioimaging and energy storage.

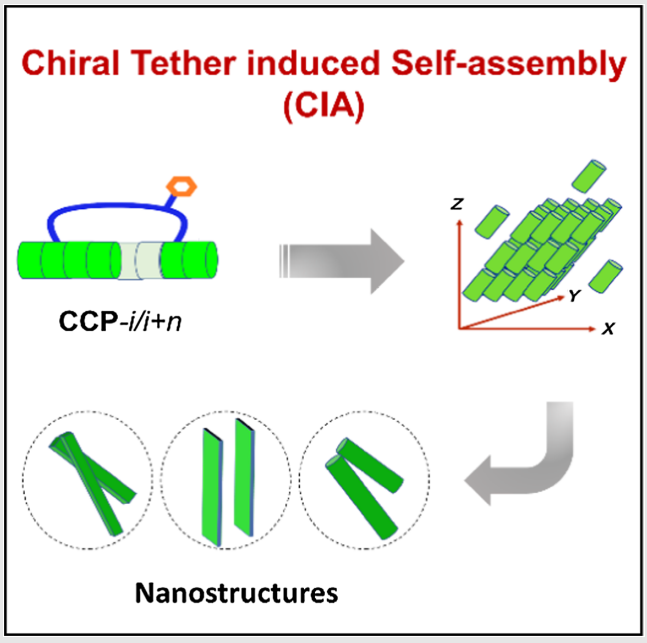

Keywords: cyclic peptide, self-assembly, chiral center, ring size, nanostructure, supramolecules, supercapacitor

DOI: 10.31635/ccschem.019.201900047
CCS Chem. **2020**, *2*, 42–51

Introduction

Self-assembly, by nature, is ubiquitous and considered a bottom-up strategy for fabricating nanomaterials.[1,2] Peptide molecules are excellent building blocks for tunable, hierarchical self-assembly due to their numerous possible sequences, diverse conformations, and rich chemical functionalities.[3,4] Commonly used building blocks for peptide self-assembly include dipeptide of phenylalanine (FF) or their derivatives,[4,5] D,L-cyclic peptides,[6] peptide amphiphiles,[7] collagens,[8] coiled coils,[9] and foldectures.[10] These materials have shown great potential for many applications, including energy storage and conversion,[11,12] optical devices,[13,14] and nanomedicine.[15,16]

The manipulation of cyclic peptide assembly is emerging as a new direction for hierarchical nanostructure fabrication.[17,18] Cyclic peptides usually possess rigid backbones and have high thermodynamic stability, compared to their linear counterparts; therefore, they are excellent building blocks for constructing advanced self-assembling architectures.[19,20] There exist two main types of self-assembly-based cyclic peptides: The first type is the widely used D,L-cyclic system, developed by Ghadiri and co-workers in 1993. The D,L-cyclic peptides assemble into hollow tubes via molecular stacking. This system has two crucial advantages: (1) tunable internal diameter[21] and (2) changeable 'external' functionality.[22] Tubular structures made by D,L-cyclic peptides assembly have been used as antibacterial agents,[23] ion channels,[24] and in molecular electronics.[25] However, the nanostructure is limited to small hollow tubes, which do not fulfill the requirements of some types of nanotechnologies, such as polarized nanorods and microrods for piezoelectronics[26] and nanogenerators,[11] or peptide vesicles and membranes for optical chiroptics, chiral sensing, and separation.[27,28] To overcome these limitations, the second type of self-assembly based on constrained all-L-cyclic or all-R-cyclic peptides was developed. One of the advantages of this latter group of peptides is their derivation from single L- or R-amino acids enabling them to adopt various secondary structures, such as helices, sheets, and turns, and depending on the structure of the component monomer, various nanostructures could be assembled. So far, nanostructures such as nanotubes, nanofibers, and nanowires have been reported to be assembled from constrained cyclic peptides.[18,29] However, due to the scarcity of constrained peptide assembly systems and their typically unpredictable assembly behaviors, it is arduous to deduct rules for de novo design of peptide assemblies based on single L- or R-cyclic peptides.

To create a novel all-L-α-cyclic peptide assembling platform, we invented an in-tether chiral center–induced peptide self-assembly (CIA) system,[18] dominated by in-tether substitutional group, with the configuration of the chiral center being the determinant of the secondary structure of the peptides, and an aromatic substitutional group

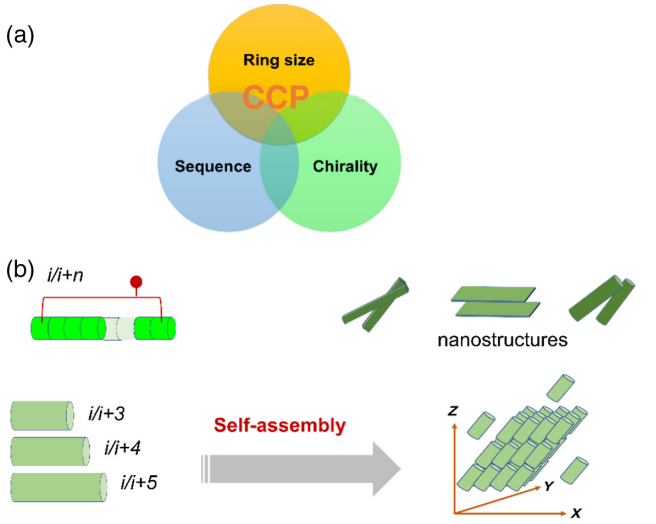

Figure 1 | *Conceptual design of self-assembly of CCP. (a) Three factors determine the topological space of CCPs. (b) Schematics of tuning peptide assembly by varying the ring size. The* i *and* i+n *represent the residue positions for cyclization.*

providing the driving force of the self-assembly. Additionally, we have demonstrated that the CIA system could be applied to different peptide sequences. However, to make the CIA system a global platform for cyclic peptide assembly, it must be tested in peptides with different ring sizes (Figure 1a). In our previous study, we showed that the CIA system was feasible with helical *i*/*i*+4 peptides. Nonetheless, it was unclear whether this method is applicable in other peptides with different ring sizes. Here, we studied the ring size effects on the assembling behavior of the CCP peptides (Figure 1b) to establish the relationship between ring size and self-assembly. Our study has provided insights into the molecular interactions of cyclic peptide assemblies. In previous endeavors, the design of the de novo peptide assembly structures remained impeded by a lack of new designs for assembling building blocks. Thus, this study might provide a promising solution through the design of CCP-assembling sequences.

Experimental Methods

Peptide self-assembly

For assembling study, the lyophilized peptide powders were dissolved in deionized (DI) water with assigned concentration. The concentrated peptide solutions were sonicated for 10 min, and then the peptide solutions were examined for self-assembly.

CD spectroscopy measurements

The peptides were dissolved in 300 μL ddH_2O to 0.10 mM final concentration. Then, we employed the Chirascan

DOI: 10.31635/ccschem.019.201900047
CCS Chem. **2020**, *2*, 42–51

Plus CD Spectrometer (Applied Photophysics Ltd, Leatherhead, United Kingdom), set at 20 °C to record the circular dichroism (CD) spectra of the peptides. The parameters used for the CD studies were as follows: wavelengths = 190–250 nm; resolution = 0.5 nm; scan speed = 0.5 nm/s. Each of the samples was scanned twice, and the averaged spectrum was smoothed using the Pro-Data Viewer by Applied Photophysics with a smooth window of 10.

X-Ray diffraction measurements

The CCP peptide nanomaterials were mounted in a vertical position onto the goniometer using a Gemini X-ray diffractometer (Oxford Instruments, Abingdon, United Kingdom) equipped with a Sapphire 3 charge-coupled device detector, with a sample-to-detector distance of 45 mm. CLEARER software (a free program, L.C. Serpell et al., *J. Appl. Crystallorg.*, 2007, 40, 966–972) was utilized as a sharpness monitor to reduce the data in two-dimension into intensity profiles in one-dimension. The peptide structures obtained from the samples were studied employing an X-ray diffractometer (XRD; PANalytical X'Pert Pro, Almelo, The Netherlands) with a Cu Kα radiation. The powder obtained from each sample was scanned in the range of 2q = 2°–60° with a step size of 0.02°.

Transmission electron microscopy

Samples (10 mL) of the peptide assemblies were sonicated for 5 s using a bath sonicator. Subsequently, the samples were placed on Formvar/carbon mesh 400 copper grids (Electron Microscopy Sciences, Hatfield, PA) for 20 s, followed by removal with nitrocellulose papers. Then the Cu grids were allowed to dry at room temperature (RT). Transmission electron microscopy (TEM) images were recorded using a high-resolution TEM (JEM-100 F, 200 kV; JEOL, Peabody, MA).

Scanning electron microscopy

Each of the pentapeptide samples was placed on silicon slides and allowed to dry at RT. Then, the samples were viewed using an scanning electron microscopy (SEM) (ZEISS Supra 55, 20 kV; Oxford Instruments X-Max 20 $mm^{2)}$.

Atomic force microscopy

Pentapeptide solutions were prepared at 5 mg/mL concentration using water (ddH_2O) as the diluent. A droplet of each solution was placed on a siliconized glass for >30 min to allow solvent volatilization. Large areas of the dried samples were imaged at varying magnifications by Axio optical microscopy (Carl Zeiss Axio Scope Imager, Jena, Germany). Atomic force microscopy (AFM) analysis was performed using a Bruker AFM multimode (MultiMode 8; Bruker, Billerica, MA). The probes used for the AFM were 40 N/m antimony (Sb) doped (*n*) silicon (Si) cantilevers with a spring constant and a resonance frequency of 300 kHz (Bruker, Shanghai, China). We carried out observations using a scan rate of 0.9 Hz at a tapping mode. After the acquisition of the AFM images, the pentapeptide data were analyzed using the Nano-Scope Analysis program (Bruker, Billerica, MA).

Peptides characterization by photoluminescence

We performed photoluminescence/photoluminescence excitation (PL/PLE) measurements of the peptide nanofibers using the Horiba FL3-11 spectrofluorimeter (Jobin Yvon Inc., Shanghai, China). The PL/PLE measurements of both peptide nanofibers and the monomers were taken using a standard cuvette, and the fluorescence measurements of the peptide nanofiber films were acquired on glass coverslips.

UV–Visible spectroscopic measurements

We obtained UV–visible spectra using an MCPD 7000 UV–visible spectrophotometer (Otsuka Electronics, Tokyo, Japan) equipped with fiber optics, an ultra-high-sensitive charge-coupled device, and an array cooled Peltier device. The sample environment was custom-made with a dark box for versatile measurements, including LB film transmission performance assessments. The transmitted light was gathered via an integral sphere, and a quartz plate, purchased from Hangzhou Shalom supplies (Hangzhou, China), was used for visible spectrometric measurements.

Preparation of PET@Au/peptide electrode and electrochemical measurements

A large photoinduced electron transfer (PET) substrate was coated with 20 nm Au film by using a DC magnetron sputtering system (Denton Vacuum, Beijing, China). Then, the coated PET was cut into small regular pieces, from which active ink materials were prepared as follows: (1) An amount of 2 mg of the peptide was dispersed in 1 mL of deionized (DI) water. (2) Nafion copolymer (Electrochemical Technology Inc., Beijing, China), 80 mL, obtained as a 5 weight percent (wt %) solution, was added, and the mixture was sonicated for 30 min to form a homogeneous ink. (3) The resultant generated ink (5 mL) was drop-casted onto the PET@Au substrate electrode, followed by air-drying. After that, we obtained a mass loading of ~1 mg/cm^2. (4) The electrode was tested using a CHI 660e electrochemical workstation (Chenhua, Shanghai, China) in three-electrode electrochemical cells using 0.05 M KH_2PO_4/0.5 M KCl or 0.1 M H_2SO_4. Pt wire and Hg/HgO were used as the counter and

DOI: 10.31635/ccschem.019.201900047
CCS Chem. **2020**, *2*, 42–51

reference electrodes, respectively. For the PET@Au/peptide electrode, the areal capacitance (F/cm^2) was calculated from the charging/discharging curves using the equation $C_V = ID_t/SD_V$, where I denotes the discharging current (A); S, the glass carbon geometrical area (cm^2), D_t, the discharging time (s), and D_V, the potential window (V). Electrochemical impedance spectroscopy (EIS) was obtained using Princeton PARSTAT 4000 (AMETEK Scientific Instruments, Shanghai, China) and employing a range of 100 kHz–0.01 Hz with an AC amplitude of 10 mV at open circuit.

Results and Discussion

Peptide synthesis and conformation analysis

To prevent perturbations from the peptide backbone on the assembly behavior of peptides, cyclic peptides, acetyl (Ac)-C(A)$_{n-1}$S$_5$(Ph)-NH$_2$ [CCP-*i*/*i*+*n*] (Figure 2a), were chosen as model peptides to investigate their self-assembling behavior. These peptides do not contain amino acid residues with significant hydrophobic interactions or hydrogen bonding features. Consequently, their peptide assembly is exclusively due to the in-tether substitutional aromatic group.[18] These CCP peptides contained the same residues for cyclization [cysteine at the N terminal and S$_5$(Ph) at the C terminal] but varied in terms of the number of residues between the cycling residues. We used the enantiomeric-pure unnatural amino acids S$_5$(R/S) to synthesize the constrained peptides.[18] Consequently, we obtained three pairs of constrained peptides, CCP-*i*/*i*+3-S/R (1-S/R), CCP-*i*/*i*+4-S/R (2-S/R), and CCP-*i*/*i*+5-S/R (3-S/R).

The peptide secondary structures were assayed using CD spectroscopy. 2-S showed an uncharacterized nonhelical conformation, and 2-R showed a helical conformation in water. Unfortunately, the initial CD spectra of 1-S/R and 2-S/R deviated from the standard curves of known conformations according to currently existing algorithms of CD (Figure 2b).[30] To overcome this challenge, we utilized the BeStSel (Beta Structure Selection; OmicX software, Seine Innopolis, Le Petit-Quevilly, France) method to estimate the secondary structures of these peptides.[31] After the user inputs the ellipticity data of the peptides, BetStSel deconvolutes the spectra into a conformation distribution, with an estimated percent prevalence of every secondary structure in the sample. Using this program, we analyzed the CD spectra and conformation distributions of the six peptides (Table 1). 1–S and 1-R are mostly in helix conformation, but the helix content of 1-S is higher than that of 1-R. 3-S is 55.5% of other conformations, probably, random coils. Moreover, 55.2% of the peptides of 3-R was in antiparallel conformation, while 2-R was estimated to be 100% helix, and 2-S was, on average, random coils (54.6%). These results were highly consistent with previous experiments,[32] indicating excellent reliability of this program for the analyses of the secondary structure of CCP peptides.

Self-assembly and morphology characterization

Accordingly, we sought to investigate the self-assembly behavior of CCP peptides. Since their appropriate concentration is pivotal for triggering self-assembly, we examined peptide concentrations ranging from 2 to

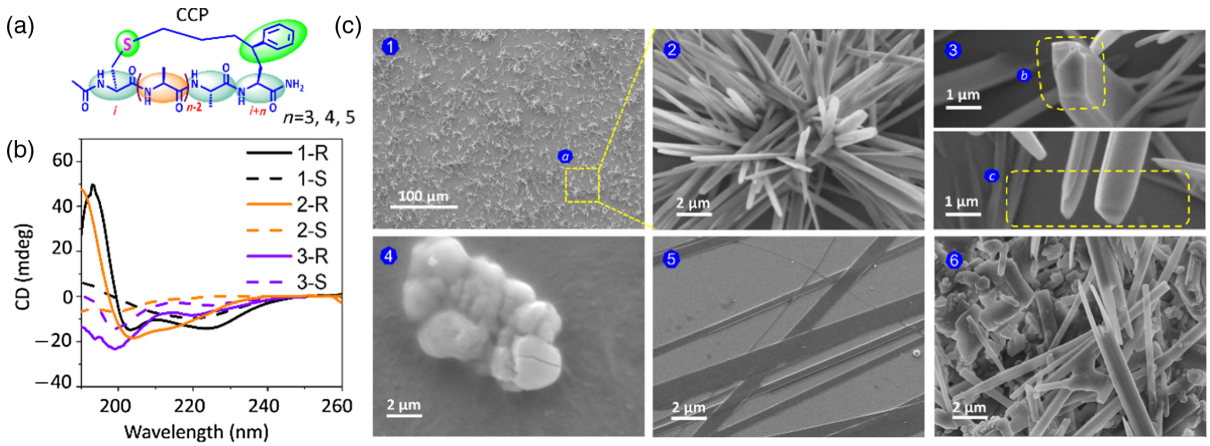

Figure 2 | *CCP conformation and assembled structures. (a) Representative chemical structure of CCP. (b) CD spectra of CCP peptides in H_2O, obtained at 20 °C. (c) SEM images of assemblies by peptide 1-S (1–3), 1-R (4), 2-R (5), and 3-R (6). Figure 2 depicts an enlarged view of the selected area (represented by a yellow dashed box* a*) in picture 1. Image 3 (up) is a perpendicular view of the end of one nanorod, indicating that the nanorod is solid (represented by a yellow dashed box* b*). Image 3 (bottom) is a side view of the end of the nanorods, suggesting a slender shape of the end of the nanorods (represented by a yellow dashed box* c*).*

DOI: 10.31635/ccschem.019.201900047
CCS Chem. **2020**, *2*, 42–51

Table 1 | *Conformation Distribution of CCP-1,2,3-S/R.*

	Helix	Antiparallel	Parallel	Turn	Others
1-S	79.4	–	–	20.6	-
1-R	36.2	26.7	7.4	7.6	22.1
2-S	6.7	25.3	–	13.4	54.6
2-R	100	–	–	–	–
3-S	22.1	55.2	–	–	22.7
3-R	9.7	22.5	–	9.3	55.5

All numbers mean percentage. The value is generated by BeSt-Sel based on the CD data.

8 mg/mL at RT, using water as the solvent/diluent. We observed that all of the peptides completely dissolve when the concentration was <2 mg/mL, indicating no self-assembly. However, at concentrations >2 mg/mL, some of the peptides tended to form a suspension, indicating the presence of insoluble species. Upon further increasing the concentration to 5 mg/mL, all of the peptides formed insoluble species. In order to achieve the optimum concentrations required for self-assembly, we made supersaturated peptide solutions at >5 mg/mL and observing the self-assembly process.

In addition to examining their thermodynamics, the assembly kinetics of the peptides was considered another critical factor that drives the programmable assembling process of peptides.[33] Kinetics are especially crucial at the initial stage of the assembly. Therefore, the samples were sonicated for 10 min to facilitate assembly. During the sonication, some of the solutions gradually became turbid. Four out of the six peptides samples, 1-S, 1-R, 2-R, and 3-R, showed visible suspended solids under an optical microscopic view (Supporting Information Figures S1). The other two samples, 2-S and 3-S, showed no such assemblies. These results might be attributable to the secondary structures assumed by the CCP peptides. The 2-S and 3-S peptides mostly adopted random coil conformations, which are unfavorable for assembly.[34] The other CCP peptides were in either helical or antiparallel conformations, which are typical conformations adopted in peptide assemblies.

Further, we performed SEM to inspect the morphology of the suspended solids. As shown in Figure 2c–1, 2, and 3, peptide 1-S adopted a rod-like morphology with diameters ranging from tens to several hundreds of nanometers (nm) and lengths in the tens of microns (μ). High-magnification SEM images revealed an ordered angular square shape of the rod structures. Moreover, the rods were solid rather than hollow tubes (Figure 2c–3). In contrast, 1-R formed amorphous aggregations (Figure 2c–4), which might have been caused by its unstable secondary structures (Table 1). Peptide 2-R assembled mostly into nanotubes or nanobelts (Figure 2c–5), consistent with previous results.[18] 3-R formed truncated tubular structures. Undoubtedly, the fragile nature of these nanomaterials was caused mainly by the relatively weak intermolecular interactions. So far, we have demonstrated that the CIA could apply to nonhelical peptides with different ring sizes and that the assembled structures were comodulated by ring size and the in-tether chiral configurations.

Then morphology of the assembled structures was characterized in detail by further imaging using TEM. The TEM images verified the observations from SEM that

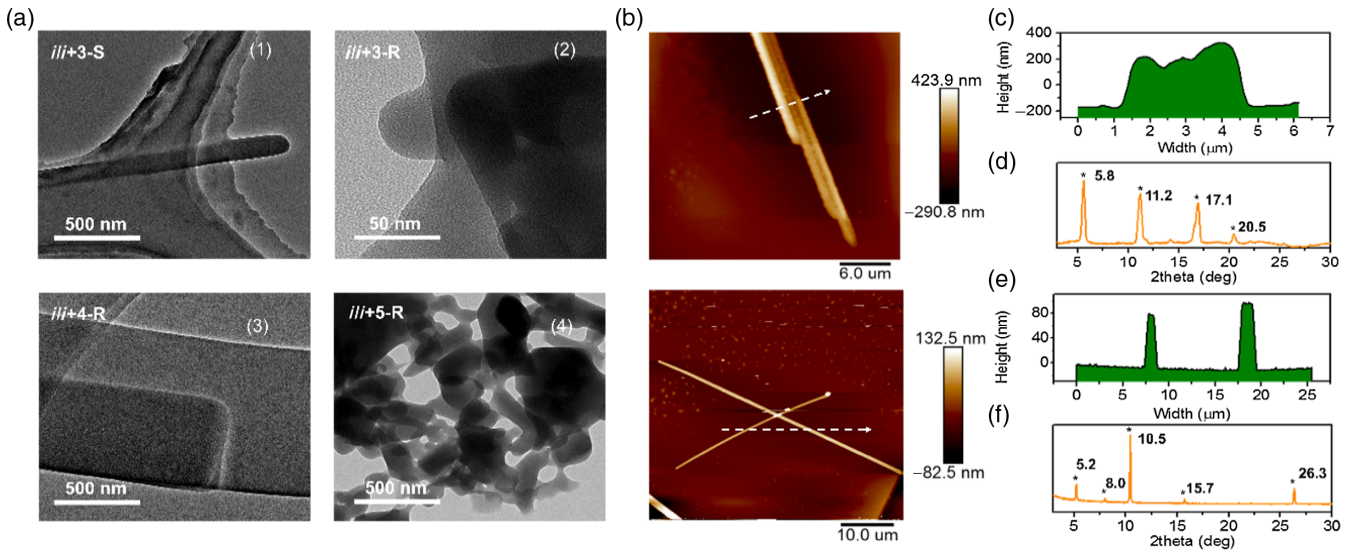

Figure 3 | *Characterization of self-assembled nanomaterials. (a) High-resolution TEM images of 1-S/R, 2-R, and 3-R peptide assemblies. (b) AFM images of peptides 1-S and 2-R assemblies. (c, e) Sectional height plots along with the labeled arrows in B, respectively. (d, f) The powder XRD pattern of 1-S and 2-R peptides assemblies, respectively.*

DOI: 10.31635/ccschem.019.201900047
CCS Chem. **2020**, *2*, 42–51

the 1-S and 2-R assemblies were tubular structures, and 1-R and 3-R were irregular shapes (Figure 3a). The stacked-layer structures of 1-S and 2-R implied that the hierarchical assembly preferred in-the-plane rather than nucleation to form nanospheres or nanoparticles. The uniform structures of the 1-S and 2-R assemblies rendered them appropriate materials for comparison in detail. AFM was performed to gain insight into the structure of the peptides; the images showed a rod-like shape of the 1-S assemblies and slender tube/needle shape of the 2-R assemblies, which were in good agreement with the SEM figures (Figure 3b). The section plots analysis of the nanopeptides to monitor height and diameter variations provided information about the size of the nanomaterials. Peptide 1-S nanorods possessed an average height of ~300 nm (Figure 3c). The peptide 2-R nanotubes were estimated to be 100 nanometers (nm) in height and tens to hundreds of microns (μm) in length (Figure 3e). The large aspect ratio of those nanostructures implied that the growth kinetics preferred the axial direction.[35]

The assemblies were examined further by powder X-ray diffraction (XRD). The diffraction peaks appeared at 5.8°, 11.2°, 17.1°, and 20.5° for 1-S assemblies (Figure 3d) and at 5.2°, 8.0°, 10.5°, 15.7°, and 26.3° for 2-R assemblies (Figure 3f), which could be attributable to the lattice spacing of the assemblies. The diffraction peaks in both of the assemblies were sharp and intense, indicating a highly crystalline material. Almost no impurity peaks were observable, confirming the high purity of the two peptide assemblies.

Optical characterization of peptide assemblies

We investigated the molecular interactions in the peptide 1-S and 2-R assemblies using UV–vis spectroscopy and fluorescence spectrophotometry. The UV–vis spectra showed a broad absorption range, from 230 to 600 nm for peptide 1-S. The absorbance of 1-S was stronger than that of 2-R at the same concentration, indicating stronger interactions between the stacked aromatic groups

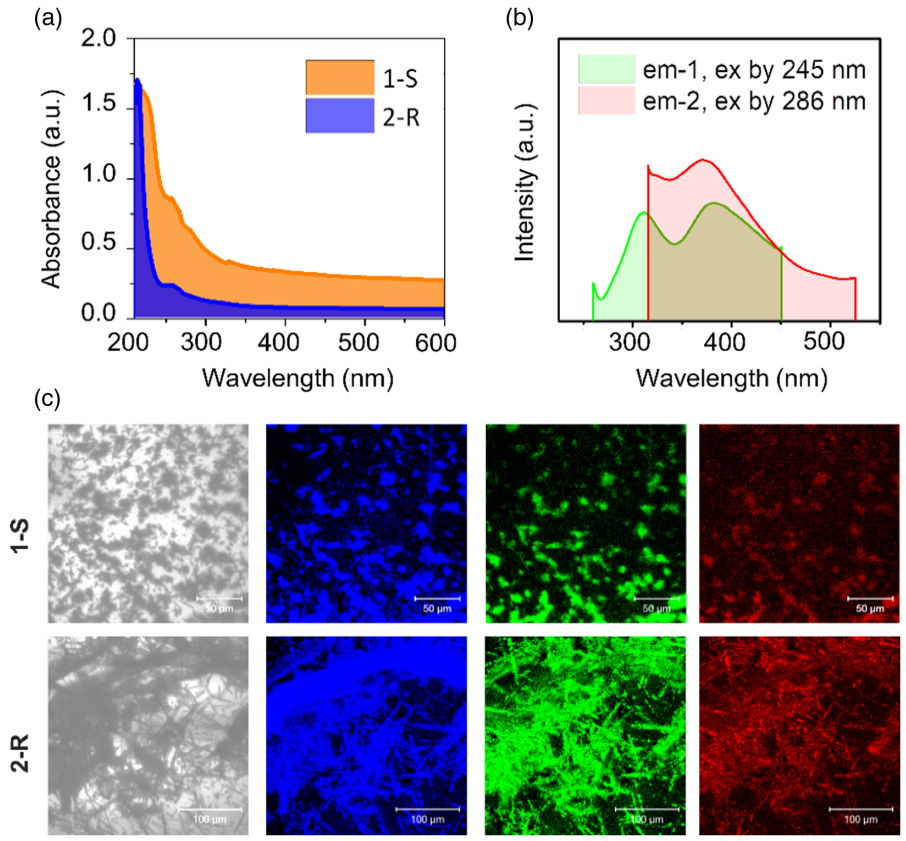

Figure 4 | *Optical study of CCP assemblies. (a) UV–Vis absorbance spectra of peptide 1-S and 2-R assemblies. a.u., arbitrary units. (b) Photoluminescence emission spectra of 1-S assemblies dispersed in water (2 mg/mL, 20 °C). The green area (em-1) represents the emission curve when a 245 nm excitation light was used. The red area (em-2) represents the emission curve when a 286 nm excitation light was used. The dashed lines represent the excitation (c) Optical and fluorescence image of 1-S and 2-R. The visible luminescence was obtained by using UV-blue, blue-green, and green-red filters, respectively.*

DOI: 10.31635/ccschem.019.201900047
CCS Chem. **2020**, *2*, 42–51

(Figure 4a).[18,36] The fluorescence spectrophotometer was used to measure the photoluminescence of the assemblies. The emission wavelength of the 1-S assemblies spanned from the UV to the visible region, em-1 and em-2, from 260 to 520 nm (Figure 4b), a similar emission profile to that of 2-R.[18] This wide range of emission (the area covered by the green and red lines) indicated that the electron delocalization was significant, which suggested strong π–π stacking interactions in the assembly and the formation of *J*-aggregates.[37,38]

Fluorescence microscopy imaging was performed using standard UV-blue, blue-green, and green-red filters for detecting emissions (Figure 4c). The results show that, with a suitable excitation wavelength, the 1-S and 2-R assemblies were able to emit blue, green, or red fluorescence. The photoluminescence of the CCP assemblies at a broad range wavelengths makes them promising materials for bio-optical and bioimaging applications.

Application of peptide assemblies in a supercapacitor

The use of peptide materials in supercapacitors (SCs) has attracted tremendous attention.[18,39] Constrained peptides display superior chemical and thermal stability, compared to their linear counterparts, making them excellent candidates for peptide-based SCs. However, the performance of peptide-based SCs is still far behind that of their inorganic counterparts, revealed by their comparatively low power and energy densities, and their long-term cycling stability is also a concern. High-performance peptide-based SCs are yet to be achievable, despite methods such as atomic layer deposition showing some promise of enhanced performance of peptide electrodes.[40] The slow development of peptide-based SCs is likely caused by a lack of theoretical rules to guide research in this area. Therefore, investigation of the correlation between peptide structure and their energy storage capacity is necessary, as it could provide fundamental knowledge to enlighten SC design. The CCP-based CIA system, which has been demonstrated applicable to peptides with variable sequence, conformation, and ring size, is a suitable platform for such investigations.

The electrochemical performance of SCs based on peptide 1-S and 2-R assemblies were investigated (Figure 5a). The tests were performed according to previously described methods.[18,40] Cyclic voltammetry (CV) measurements were obtained using a three-electrode cell in 0.05 M KH_2PO_4 + 0.5 M KCl electrolyte at RT. The CV curves of the electrodes were based on 1-S, or 2-R peptide assemblies obtained at scan rates ranging from 10 to 80 mV/s at a voltage range of –0.5 to 0.5 V, using Hg/HgO as a reference electrode (Supporting Information Figures S2). We calculated the specific areal capacitance by integrating over the full CV curves to determine the average value (Figure 5b and Supporting Information Figures S3). Peptide 2-R-based electrode delivered an areal capacitance of 3.0 mF/cm^2

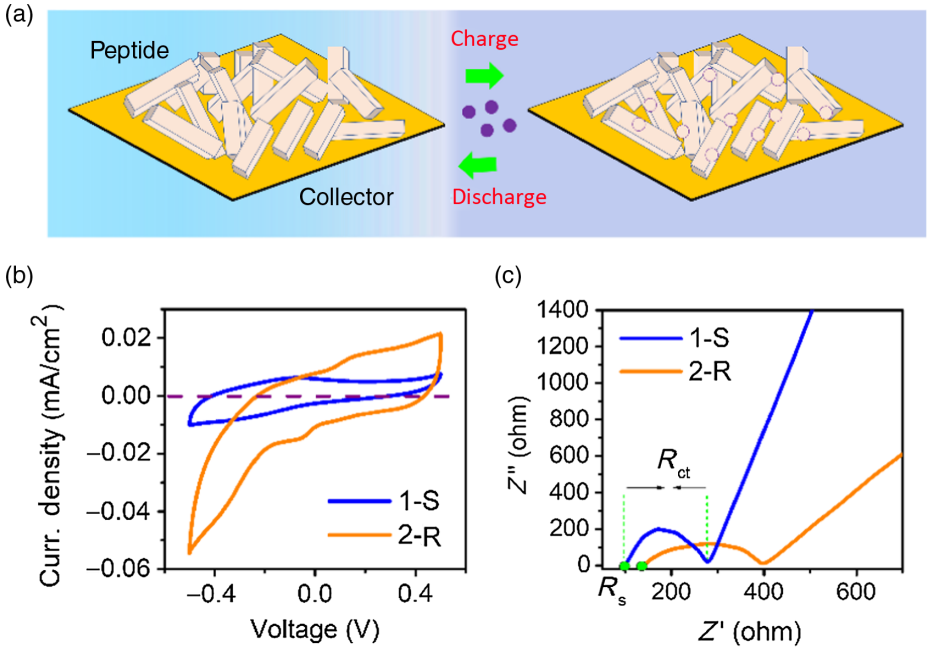

Figure 5 | *Application of peptide assemblies in SCs. (a) Schematic illustration of the peptide-based electrodes. (b) Cyclic voltammograms at 10 mV/S for 1-S and 2-R assemblies-based electrodes, respectively. (c) Nyquist plots of the peptide electrodes at open circuit potential with 10 mV amplitude between 0.01 Hz and 100 KHz.*

DOI: 10.31635/ccschem.019.201900047
CCS Chem. **2020**, *2*, 42–51

at 10 mV/S and 1.3 mF/cm^2 at 80 mV/S. In contrast, electrode based on peptide 1-S exhibited a lower areal capacitance, showing only 0.9 mF cm^{-2} at 10 mV/S and 0.45 mF/cm^2 at 80 mV/S.

To investigate the difference in specific capacitance, we performed an EIS study of the peptide-based electrodes.[41] Nyquist plots obtained from the analysis are shown in Figure 5c. The equivalent series resistances (R_s) were approximately 98 and 140 ohms for 1-S and 2-R electrodes, respectively. Additionally, the charge-transfer resistance (R_{ct}) of the 1-S electrode was ~89 ohms, much lower than that of 2-R (128 ohms). These results suggested that electrode 1-S had a superior charge-transfer capability and closer contact between the peptide nanostructures and the collector than 2-R.[40,42,43] Moreover, the lines in the low-frequency range of 1-S displayed a slope greater than those in 2-R, suggesting good capacitive behavior with less ion diffusion retardation. The EIS results appear to contradict the CV measurements. This might be explained by the comodulation of the performance of the peptide-based SC by several factors, including electrical conductivity of the materials, available surface area, and accessible wettability of the nanomaterials. Although the conductivity of 1-S was better than that of 2-R, the surface area for ion absorption of 1-S was much less than that of 2-R, as both hollow tubes and solid tubes exist in the 2-R assembly[18], contrary to the only solid nanorods present in 1-S. Additional details about the energy storage mechanism warrant further investigation.

Since the compelling first demonstration of cyclic DL-α-cyclic peptide assembly into a hollow tubular structure via the stacking of DL-cyclic rings by Ghadiri et al. in 1993,[44] the applications of these materials has been expanded in chemistry[45], biochemistry,[46,47] and material science.[48,25] One of the advantages of cyclic DL-peptide nanotubes with respect to their β-helical counterparts is the ability to control the internal diameter of the nanotube rigorously by simply varying the size of the peptide ring.[21] However, their planar structure prevents diversified assembly into tertiary structures other than hollow tubules. Accordingly, other cyclic peptide systems for self-assembly have recently attracted much attention, including that of the all L-α-cyclic peptide. The design of cyclic peptide assemblies based on the all-L-α-cyclic peptides is a synthetic challenge due to the massive entropy loss during the cycling, and the assembling process demands a significant driving force for molecular packing. Currently, most investigative efforts are relying on exploiting the assembling of cyclic peptides that adopt β-sheet or α-helix conformation.[29,49] However, the majority of those systems are sequence size- or ring-size-dependent and represent a limited potential for constructing various nanostructures. In this study, we have further explored our previously published CIA system by studying the relationship between ring size and self-assembly behavior. We confirm that the CIA approach is generally applicable to different sequences, conformations, and ring sizes, rendering it a versatile platform for fabricating peptide assemblies.

Conclusions

We have synthesized a library of CCPs and studied their conformation and assembly behavior and discovered that the peptide assemblies possessed intriguing photoluminescence and electrochemical properties. The results described herein demonstrate for the first time that constrained cyclic peptides with different ring sizes could self-assemble into different nanostructures. A noteworthy feature of the CCP system is good tolerance of different secondary structures, ring size, and peptides sequences. Based on this system, a variety of nanostructures could be constructed, which display variable physical properties, rendering it a versatile platform for molecular interaction studies and comparative investigations of the structure–performance relationship of peptide assemblies. Furthermore, we have acquired some ability to predictably design and synthesize peptide assemblies with desirable properties using the CIA system, although we have not yet solved the assembly mechanism of those assemblies. We envision that the functional materials made by the CIA system might have broad applications in chemistry, biology, and engineering. Future work would focus on uncovering the molecular packing mechanisms in these assemblies.

Supporting Information

Supporting Information is available.

Conflicts of Interest

The authors declare no conflict of interest.

Acknowledgments

We acknowledge financial support from the Natural Science Foundation of China (grant nos. 21778009, 21801019, 21977010, 81701818, and 51803006) and the Shenzhen Science and Technology Innovation Committee (nos. JCYJ20170817172023838 and JCYJ20180507181527112).

References

1. Ulijn, R. V.; Smith, A. M. Designing Peptide Based Nanomaterials. *Chem. Soc. Rev.* **2008**, *37*, 664–675.

2. Adler-Abramovich, L.; Gazit, E. The Physical Properties of Supramolecular Peptide Assemblies: From Building Block Association to Technological Applications. *Chem. Soc. Rev.* **2014**, *43*, 6881–6893.
3. de la Rica, R.; Matsui, H. Applications of Peptide and Protein-Based Materials in Bionanotechnology. *Chem. Soc. Rev.* **2010**, *39*, 3499–3509.
4. Gazit, E. Self-Assembled Peptide Nanostructures: The Design of Molecular Building Blocks and Their Technological Utilization. *Chem. Soc. Rev.* **2007**, *36*, 1263–1269.
5. Yan, X.; Zhu, P.; Li, J. Self-Assembly and Application of Diphenylalanine-Based Nanostructures. *Chem. Soc. Rev.* **2010**, *39*, 1877–1890.
6. Chapman, R.; Danial, M.; Koh, M. L.; Jolliffe, K. A.; Perrier, S. Design and Properties of Functional Nanotubes From the Self-Assembly of Cyclic Peptide Templates. *Chem. Soc. Rev.* **2012**, *41*, 6023–6041.
7. Barclay, T. G.; Constantopoulos, K.; Matisons, J. Nanotubes Self-Assembled from Amphiphilic Molecules via Helical Intermediates. *Chem. Rev.* **2014**, *114*, 10217–10291.
8. Tanrikulu, I. C.; Forticaux, A.; Jin, S.; Raines, R. T. Peptide Tessellation Yields Micrometre-Scale Collagen Triple Helices. *Nat. Chem.* **2016**.
9. Joh, N. H.; Wang, T.; Bhate, M. P.; Acharya, R.; Wu, Y.; Grabe, M.; Hong, M.; Grigoryan, G.; DeGrado, W. F. De Novo Design of a Transmembrane Zn^{2+}-Transporting Four-Helix Bundle. *Science* **2014**, *346*, 1520–1524.
10. Yoo, S. H.; Lee, H.-S. Foldectures: 3D Molecular Architectures from Self-Assembly of Peptide Foldamers. *Acc. Chem. Res.* **2017**, *50*, 832–841.
11. Nguyen, V.; Zhu, R.; Jenkins, K.; Yang, R. Self-Assembly of diphenylalanine Peptide with Controlled Polarization for Power Generation. *Nat. Commun.* **2016**, *7*, 13566.
12. Tao, K.; Makam, P.; Aizen, R.; Gazit, E. Self-Assembling Peptide Semiconductors. *Science* **2017**, *358*, eaam9756.
13. Amdursky, N.; Molotskii, M.; Aronov, D.; Adler-Abramovich, L.; Gazit, E.; Rosenman, G. Blue Luminescence Based on Quantum Confinement at Peptide Nanotubes. *Nano Lett.* **2009**, *9*, 3111–3115.
14. Ryu, J.; Lim, S. Y.; Park, C. B. Photoluminescent Peptide Nanotubes. *Adv. Mater.* **2009**, *21*, 1577–1581.
15. Ross, J. F.; Bridges, A.; Fletcher, J. M.; Shoemark, D.; Alibhai, D.; Bray, H. E. V.; Beesley, J. L.; Dawson, W. M.; Hodgson, L. R.; Mantell, J.; Verkade, P.; Edge, C. M.; Sessions, R. B.; Tew, D.; Woolfson, D. N. Decorating Self-Assembled Peptide Cages with Proteins. *ACS Nano* **2017**, *11*, 7901–7914.
16. He, H.; Zheng, N.; Song, Z.; Kim, K. H.; Yao, C.; Zhang, R.; Zhang, C.; Huang, Y.; Uckun, F. M.; Cheng, J.; Zhang, Y.; Yin, L. Suppression of Hepatic Inflammation via Systemic siRNA Delivery by Membrane-Disruptive and Endosomolytic Helical Polypeptide Hybrid Nanoparticles. *ACS Nano* **2016**, *10*, 1859–1870.
17. Mondal, S.; Adler-Abramovich, L.; Lampel, A.; Bram, Y.; Lipstman, S.; Gazit, E. Formation of Functional Super-Helical Assemblies by Constrained Single Heptad Repeat. *Nat. Commun.* **2015**, *6*, 8615.
18. Hu, K.; Jiang, Y.; Xiong, W.; Li, H.; Zhang, P.-Y.; Yin, F.; Zhang, Q.; Geng, H.; Jiang, F.; Li, Z.; Wang, X.; Li, Z. Tuning Peptide Self-Assembly by an In-Tether Chiral Center. *Sci. Adv.* **2018**, *4*, eaar5907.
19. Hill, T. A.; Shepherd, N. E.; Diness, F.; Fairlie, D. P. Constraining Cyclic Peptides to Mimic Protein Structure Motifs. *Angew. Chem. Int. Ed.* **2014**, *53*, 13020–13041.
20. Mondal, S.; Gazit, E. The Self-Assembly of Helical Peptide Building Blocks. *ChemNanoMat* **2016**, *2*, 323–332.
21. Hourani, R.; Zhang, C.; Van Der Weegen, R.; Ruiz, L.; Li, C.; Keten, S.; Helms, B. A.; Xu, T. Processable Cyclic Peptide Nanotubes with Tunable Interiors. *J. Am. Chem. Soc.* **2011**, *133*, 15296–15299.
22. Xu, T.; Zhao, N.; Ren, F.; Hourani, R.; Lee, M. T.; Shu, J. Y.; Mao, S.; Helms, B. A. Subnanometer Porous Thin Films by the Co-Assembly of Nanotube Subunits and Block Copolymers. *ACS Nano* **2011**, *5*, 1376–1384.
23. Montero, A.; Gastaminza, P.; Law, M.; Cheng, G.; Chisari, F. V.; Ghadiri, M. R. Self-Assembling Peptide Nanotubes with Antiviral Activity Against Hepatitis C Virus. *Chem. Biol.* **2011**, *18*, 1453–1462.
24. Montenegro, J.; Ghadiri, M. R.; Granja, J. R. Ion Channel Models Based on Self-Assembling Cyclic Peptide Nanotubes. *Acc. Chem. Res.* **2013**, *46*, 2955–2965.
25. Ashkenasy, N.; Horne, W. S.; Ghadiri, M. R. Design of Self-Assembling Peptide Nanotubes with Delocalized Electronic States. *Small* **2006**, *2*, 99–102.
26. Kholkin, A.; Amdursky, N.; Bdikin, I.; Gazit, E.; Rosenman, G. Strong Piezoelectricity in Bioinspired Peptide Nanotubes. *ACS Nano* **2010**, *4*, 610–614.
27. Wang, Y.; Qi, W.; Huang, R.; Yang, X.; Wang, M.; Su, R.; He, Z. Rational Design of Chiral Nanostructures from Self-Assembly of a Ferrocene-Modified Dipeptide. *J. Am. Chem. Soc.* **2015**, *137*, 7869–7880.
28. Chen, X.; He, Y.; Kim, Y.; Lee, M. Reversible, Short α-Peptide Assembly for Controlled Capture and Selective Release of Enantiomers. *J. Am. Chem. Soc.* **2016**, *138*, 5773–5776.
29. Sim, S.; Kim, Y.; Kim, T.; Lim, S.; Lee, M. Directional Assembly of Alpha-Helical Peptides Induced by Cyclization. *J. Am. Chem. Soc.* **2012**, *134*, 20270–20272.
30. Greenfield, N. J. Using Circular Dichroism Spectra to Estimate Protein Secondary Structure. *Nat. Protoc.* **2006**, *1*, 2876.
31. Micsonai, A.; Wien, F.; Kernya, L.; Lee, Y. H.; Goto, Y.; Refregiers, M.; Kardos, J. Accurate Secondary Structure Prediction and Fold Recognition for Circular Dichroism Spectroscopy. *Proc. Natl. Acad. Sci. U.S.A.* **2015**, *112*, E3095–3103.
32. Hu, K.; Geng, H.; Zhang, Q.; Liu, Q.; Xie, M.; Sun, C.; Li, W.; Lin, H.; Jiang, F.; Wang, T.; Wu, Y.-D.; Li, Z. An In-tether Chiral Center Modulates the Helicity, Cell Permeability, and Target Binding Affinity of a Peptide. *Angew. Chem. Int. Ed.* **2016**, *55*, 8013–8017.
33. Wang, J.; Liu, K.; Xing, R.; Yan, X. Peptide Self-Assembly: Thermodynamics and Kinetics. *Chem. Soc. Rev.* **2016**, *45*, 5589–5604.
34. Pagel, K.; Koksch, B. Following Polypeptide Folding and Assembly with Conformational Switches. *Curr. Opin. Chem. Biol.* **2008**, *12*, 730–739.

DOI: 10.31635/ccschem.019.201900047
CCS Chem. **2020**, *2*, 42–51

35. Adler-Abramovich, L.; Arnon, Z. A.; Sui, X.; Azuri, I.; Cohen, H.; Hod, O.; Kronik, L.; Shimon, L. J. W.; Wagner, H. D.; Gazit, E. Bioinspired Flexible and Tough Layered Peptide Crystals. *Adv. Mater.* **2018**, *30*, 1704551.
36. Yan, X.; Li, J.; Möhwald, H. Self-Assembly of Hexagonal Peptide Microtubes and Their Optical Waveguiding. *Adv. Mater.* **2011**, *23*, 2796–2801.
37. Spano, F. C.; Silva, C. H- and J-Aggregate Behavior in Polymeric Semiconductors. *Annu. Rev. Phys. Chem.* **2014**, *65*, 477–500.
38. Li, R.; Horgan, C. C.; Long, B.; Rodriguez, A. L.; Mather, L.; Barrow, C. J.; Nisbet, D. R.; Williams, R. J. Tuning the Mechanical and Morphological Properties of Self-Assembled Peptide Hydrogels via Control Over the Gelation Mechanism Through Regulation of Ionic Strength and the Rate of pH Change. *RSC Adv.* **2015**, *5*, 301–307.
39. Adler-Abramovich, L.; Aronov, D.; Beker, P.; Yevnin, M.; Stempler, S.; Buzhansky, L.; Rosenman, G.; Gazit, E. Self-Assembled Arrays of Peptide Nanotubes by Vapour Deposition. *Nat. Nanotechnol.* **2009**, *4*, 849–854.
40. Hu, K.; Zheng, C.; An, M.; Ma, X.; Wang, L. A Peptide-Based Supercapacitor and its Performance Improvement via TiO_2 Coating. *J. Mater. Chem. A.* **2018**, *6*, 8047–8052.
41. Macdonald, J. R.; Barsoukov, E. Impedance Spectroscopy: Theory, Experiment, and Applications. *History* **2005**, *1*, 1–13.
42. Zhang, J.; Wu, X.; Gan, Z.; Zhu, X.; Jin, Y. Unidirectionally Aligned Diphenylalanine Nanotube/Microtube Arrays with Excellent Supercapacitive Performance. *Nano Res.* **2014**, *7*, 929–937.
43. Beker, P.; Rosenman, G. Bioinspired Nanostructural Peptide Materials for Supercapacitor Electrodes. *J. Mater. Res.* **2009**, *25*, 1661–1666.
44. Ghadiri, M. R.; Granja, J. R.; Milligan, R. A.; McRee, D. E.; Khazanovich, N. Self-Assembling Organic Nanotubes Based on a Cyclic Peptide Architecture. *Nature* **1993**, *366*, 324.
45. Brea, R. J.; Vázquez, M. E.; Mosquera, M.; Castedo, L.; Granja, J. R. Controlling Multiple Fluorescent Signal Output in Cyclic Peptide-Based Supramolecular Systems. *J. Am. Chem. Soc.* **2007**, *129*, 1653–1657.
46. Fernandez-Lopez, S.; Kim, H.-S.; Choi, E. C.; Delgado, M.; Granja, J. R.; Khasanov, A.; Kraehenbuehl, K.; Long, G.; Weinberger, D. A.; Wilcoxen, K. M. Antibacterial Agents Based on the Cyclic D,L-α-Peptide Architecture. *Nature* **2001**, *412*, 452.
47. Richman, M.; Wilk, S.; Chemerovski, M.; Wärmländer, S. K. T. S.; Wahlström, A.; Gräslund, A.; Rahimipour, S. In Vitro and Mechanistic Studies of an Antiamyloidogenic Self-Assembled Cyclic D,L-α-Peptide Architecture. *J. Am. Chem. Soc.* **2013**, *135*, 3474–3484.
48. Horne, W. S.; Ashkenasy, N.; Ghadiri, M. R. Modulating Charge Transfer Through Cyclic D,L-α-Peptide Self-Assembly. *Chem.–Eur. J* **2005**, *11*, 1137–1144.
49. Cheng, P.-N.; Liu, C.; Zhao, M.; Eisenberg, D.; Nowick, J. S. Amyloid β-Sheet Mimics that Antagonize Protein Aggregation and Reduce Amyloid Toxicity. *Nat. Chem.* **2012**, *4*, 927.

DOI: 10.31635/ccschem.019.201900047
CCS Chem. **2020**, *2*, 42–51